

Journal of Materials Chemistry A

Accepted Manuscript



This is an *Accepted Manuscript*, which has been through the Royal Society of Chemistry peer review process and has been accepted for publication.

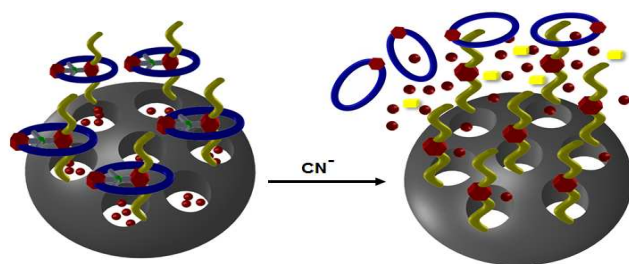
Accepted Manuscripts are published online shortly after acceptance, before technical editing, formatting and proof reading. Using this free service, authors can make their results available to the community, in citable form, before we publish the edited article. We will replace this *Accepted Manuscript* with the edited and formatted *Advance Article* as soon as it is available.

You can find more information about *Accepted Manuscripts* in the [Information for Authors](#).

Please note that technical editing may introduce minor changes to the text and/or graphics, which may alter content. The journal's standard [Terms & Conditions](#) and the [Ethical guidelines](#) still apply. In no event shall the Royal Society of Chemistry be held responsible for any errors or omissions in this *Accepted Manuscript* or any consequences arising from the use of any information it contains.

*Graphical Abstract:***A cyanide responsive supramolecular nanovalve based on Pd(II)-templated pseudorotaxane**

Mandapati V. Ramakrishnam Raju and Hong-Cheu Lin*



A nanovalve system composed of mesoporous silica nanoparticle (MSN)-based carrier mechanized with a square planar Pd(II)-templated pseudorotaxane was synthesized, which could be responsive to cyanide and follow by demetalation to release both macrocycles and sensory dyes concomitantly.

A cyanide responsive supramolecular nanovalve based on Pd(II)-templated pseudorotaxane

Cite this: DOI: 10.1039/x0xx00000x

Mandapati V. Ramakrishnam Raju and Hong-Cheu Lin*

Received
Accepted

DOI: 10.1039/x0xx00000x

www.rsc.org/

In this article, we designed and synthesized a nanovalve system composed of mesoporous silica nanoparticle (MSN)-based carrier mechanized with a square planar Pd(II)-templated pseudorotaxane, which could be responsive to cyanide and follow by demetalation to release both macrocycles and desirable porous contents (e.g. dye indicators) concomitantly. Gatekeeping of mesopore is achieved by forming an intact coordination between aqueous soluble monodentate pyridine axles and tridentate macrocycle Pd complex via a square planar metal template approach. A facile nanovalve system with an ability to work under anion stimulus condition is presented. Furthermore, anion stimulated dye releasing efficacies from Pd(II) metal template gated nanovalves are independent of pH effects, which are also successfully demonstrated utilizing luminescence spectroscopy.

Introduction

Ever since the initial report utilizing MCM-41 type mesoporous silica nanoparticles as drug delivery vehicle¹ and the inception of “magic bullet” concept² propelled the field of site-specific drug delivery systems, these epitomes have become good nanocarriers with solid supports at molecular and supramolecular levels, which are enduring to stimulate the scientific community. After the seminal discovery of mesoporous silica nanostructures (i.e., MCM-41) in early 1990s by Kuroda and Kresge,^{3,4} the ensuing two decades have witnessed revolutionary changes in their bottom-up nanotechnological approaches,⁵ thus their ease of functionalization allowed to design diverse mesoporous silica nanoparticle (MSN)-based platforms for controlled drug releasing,⁶ catalytic,⁷ sensing⁸ and diagnostic applications.⁹ The exceptional structural properties of MSNs, such as large surface areas, tunable pores, robust structures and augmented surface properties, make them as ideal candidates for hosting cargos of various sizes, shapes and functions.¹⁰ The exquisite Stimulus responsiveness, nontoxicities, modular fashioned synthetic approaches and ease of functionalization are continued to motivate chemists in designing novel theranostic devices or environmental nanoscale devices.

In addition, harnessing of mechanostereochemistry by functionalizing mesoporous silica nanoparticles with mechanically interlocked molecules (MIMs) has changed the fate of delivery systems owing to their reversible and controllable molecular switching capability in delivering cargos

of interests efficiently at the desired sites under specific stimuli. Thus, both supramolecular and molecular versions of theranostic nanodevices based on mechanized mesoporous silica nanoparticles (MSNPs) are highly investigated,^{11,12,13} as their action reminiscent of the action of a linear motor. A nanovalve is a machine fabricated by combining a movable part threaded through axle unit with a covalent attachment to solid nanoparticle support at pore openings. Thus, in order to generate an intelligent nanovalve the mechanical binding event between movable parts and thread unit should be ideal enough to work under desired temporary quelling conditions to regulate the cargo releasing functions.

During the last decade, we have witnessed a variety of MSNP-based delivery systems encompassing wide ranges of capping agents. However, the majority of these nanovalves have utilized cyclodextrins,¹⁴ cucurbiturils,¹⁵ crown ethers,¹⁶ calixarenes¹⁷ and pillar[5]arene¹⁸ as gate keeper units to facilitate on-command cargo releasing functions. Zink *et al* have demonstrated a metal-latched nanovalve system for the controlled cargo release.¹⁹ Du *et al* reported that the delivery efficacies could be tuned by synergetic gating of metal-latching ligands and metal-chelating proteins to mesoporous silica nanovehicles.²⁰ Recently Wu *et al* reported a Pd(II) metal-template capped rotaxane nanovalve as a folic acid mediated cancer-targeted drug delivery system based on commonly encountered redox trigger.²¹ Nanovalves have long been triggered under light,^{14b,14h,15c,17b} pH,^{14c,15a-d,16a-b,18a} competitive binding,^{16b,18a} redox^{14c,14e,21} and enzymatic stimulus^{14a,17a,18b} events. These events subsequently regulate the mechanical motions of movable component over the tethered stalk in a back and forth fashion to release the encapsulated cargo at specific sites.

Myriads of vital biological reactions, photo synthetic processes, enzymatic reactions, ion-channel transportations and neurotransmissions are governed by metals and anions.²² On account of nature of non-covalent interactions between matching

Department of Materials Science and Engineering, National Chiao Tung University, Hsinchu 30049, Taiwan. Email: linhc@mail.nctu.edu.tw.

† Electronic Supplementary Information (ESI) available: [¹H and ¹³C NMR data of organic stack, pseudorotaxane and supporting Figs. S1-S13]. See DOI: 10.1039/c000000x/

pieces, many of these nanovalves have often been limited in their use to organic solvents. Despite of these accomplishments, it remains challenging to design a nanovalve system with a metal template which could be triggered in a precisely controlled manner under aqueous anionic stimulus conditions. Thus, from the viewpoint of creating a canny nanovalve system, gate-keeping approaches with metal-templated pseudorotaxanes might provide interesting paradigms. However, to the best of our knowledge, an anion responsive metal-templated supramolecular nanovalves have not been reported previously. To mimic this, we need an ideal metal-templated pseudorotaxane system with an aqueous tolerance to work under deliberate stimulus controls.

Herein, we designed and synthesized an aqueous tolerable nanovalve system with a square planar Pd(II)-template as a gate-keeper. We chose a pyridyl thread with an aqueous soluble tail and another terminal OH so that the nanovalve could be covalently grafted to MCM-41 and operated under biological conditions. Furthermore, we used a well-established fluorescein disodium salt (FDS) as a cargo to show controlled releasing studies of the present system in solution utilizing luminescence spectroscopy. The principle of removal the metal template and concomitant escape of guest molecules from the present nanovalve system under aqueous tetrabutylammonium cyanide (TBACN) stimulus is outlined in Fig. 1.

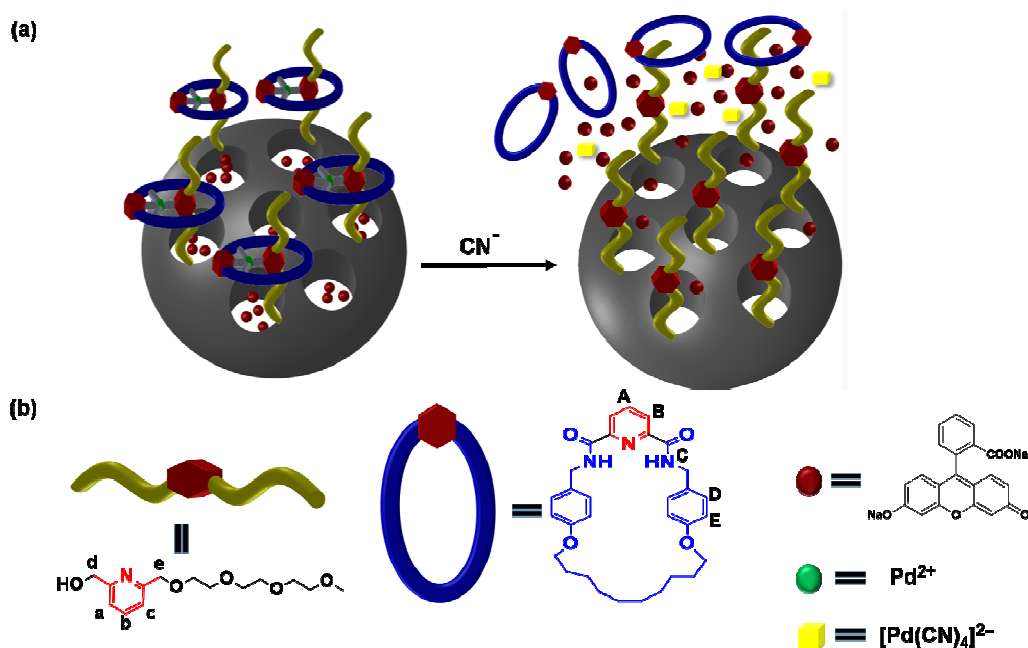


Fig. 1 (a) Graphical representation of Pd(II)-template based pseudorotaxane as a gate-keeper and its operational mechanism under cyanide stimulus. (b) Chemical structures of pyridyl stalk **3**, macrocycle, dye molecule (FDS) and resulting metal complex ($[\text{Pd}(\text{CN})_4]^{2-}$).

Experimental

General methods and materials

Reagents and chemicals were purchased from Aldrich and Fluka and were used without further purification. Solvents were freshly distilled and purified by passing through short pad alumina prior to use. Compounds **1**²³, **2**²⁴ and macrocycle ligand complex **MPd**²⁵ were synthesized according to literature procedures. UV-Vis spectra were recorded on Jasco UV-600 spectrophotometer using 1 cm quartz cuvette. Fluorescence measurements were conducted with HITACHI 7000 Series Spectrophotometer. All emission and excitation spectra were corrected for the detector responses and the lamp outputs. NMR spectra were recorded on Bruker Avance DRX300 Series (^1H : 300 MHz; ^{13}C : 75 MHz) at a constant temperature of 298 K. Chemical shifts are reported in parts per million from low to high fields and referenced to residual solvent (CDCl_3 : ^1H δ = 7.26, and ^{13}C δ = 77.23, respectively). ^{13}C and ^{29}Si cross-polarization magic-angle-spinning (CP-MAS) solid state NMR spectra were recorded on Bruker Avance 400 MHz instrument. Coupling constants (J) are reported in hertz (Hz). Elemental analyses were conducted on HERAEUS CHN-OS RAPID elemental analyser. Fourier transform infrared (FT-IR) spectroscopy data were collected using Perkin Elmer IR spectrophotometer. Solid samples were

analyzed using KBr pellet method. Nitrogen isotherms were measured using Micromeritics ASAP 2000. X-ray diffraction (XRD) analysis was performed using Bruker AXS D2 Phaser in conjunction with LENSEYE detector and $\text{CuK}\alpha$ radiation source. Field emission scanning electron microscopic (SEM) images and energy-dispersive X-ray spectroscopy (EDX) analysis were collected using a JEOL JSM-6500F apparatus with OXFORD INCA system. Transmission electron microscopy JEOL JEM-ARM 200F microscope (TEM) was used in analyzing mesoporous structures. Zeta potential measurements were carried out using Malvern Zetasizer Nano ZSP instrument. X-ray photoelectron spectroscopy (XPS) measurements were conducted using VG Scientific Micro Lab Analyser. Controlled fluorescein cargo releasing characteristics were measured using luminescence spectroscopy.

Synthesis of compound **3**

In oven dried 250 mL RBF pyridine-2,6-diylldimethanol **1** (2.5 g, 17.96 mmol, 1 equiv) was dissolved in anhydrous THF (100 mL) and the solution was applied to 3 freeze-thaw-pump cycles and stirred under N_2 atmosphere. Then sodium hydride (0.538 mg, 13.47 mmol, 0.75 equiv, 60 wt% powder) was added to the solution and heated to 55°C for 30 min. Later 2-(3-(2-methoxyethoxy)propoxy)ethyl 4-methylbenzenesulfonate compound

2 (4.86 g, 15.27 mmol, 0.85 equiv) in THF (25 mL) was added slowly in 10 min and then the resulting solution was heated to reflux for 14 h, at which time the resulting suspension was slowly cooled down to room temperature and filtered through celite bed and washed extensively with CH_2Cl_2 . The crude product was purified by flash column chromatography using $\text{CH}_2\text{Cl}_2/\text{MeOH}$ (98:2) to get the desired one-side product **3** as light brown liquid (0.85 g, 2.97 mmol, 17%), two-side product (1.65 g, 3.83 mmol, 21%) and remained **1** were recovered.

¹H NMR (300 MHz, CDCl_3 , 25°C): δ (ppm) = 7.64 (t, $J_t = 7.65$ Hz, 1H), 7.32 (d, $J_d = 7.52$ Hz, 1H), 7.14 (d, $J_d = 7.52$ Hz, 1H), 4.68 (s, 2H), 4.63 (s, 2H), 3.68-3.66 (m, 4H), 3.64-3.62 (m, 4H), 3.61-3.59 (m, 2H), 3.52-3.50 (m, 2H), 3.33 (s, 3H); **¹³C NMR** (75 MHz, CDCl_3 , 25°C): δ (ppm) = 158.7, 157.4, 137.3, 119.8, 119.1, 73.7, 71.8, 70.5, 70.4, 70.2, 64.1, 58.9; **IR** (KBr, cm^{-1}): 3434, 3032, 2906, 2104, 1978, 1645, 1536, 1450, 1332, 1264, 941; **MS (+EI)**: (m/z): Calcd for $\text{C}_{14}\text{H}_{23}\text{NO}_5$; 285.34; found: 286.3 $[\text{M}+\text{H}]^+$, **Anal.** Calcd. for $\text{C}_{14}\text{H}_{23}\text{NO}_5$: C, 58.93; H, 8.12, N, 4.91 found; C, 58.69.11; H, 8.00, N, 4.93.

Synthesis of Pseudorotaxane P1

Pyridyl stalk **3** (0.40 g, 1.40 mmol, 1.0 equiv) was taken into a 50 mL round bottomed flask containing a mixture of anhydrous $\text{CHCl}_3/\text{CH}_3\text{CN}$ (8/2, 20 mL) solvent. The solution was purged with argon for 5 min. The pre-formed macrocycle ligand complex **MPd** (0.926 g, 1.40 mmol, 1.0 equiv) was added to the above solution and stirred for 4 h at room temperature. After completion of pseudorotaxanation the solution was evaporated under reduced pressure. The crude residue was subjected to column chromatography (silica gel, $\text{CH}_2\text{Cl}_2/\text{MeOH}$: 99/1). A yellow solid **P1** was recovered (1.15 g, 1.27 mmol, 91%). Chemical formula: $\text{C}_{45}\text{H}_{58}\text{N}_4\text{O}_9\text{Pd}$, molecular weight: 905.38.; mp. 185.1-186.5°C

¹H NMR (300 MHz, CDCl_3 , 25°C): δ (ppm) = 8.13 (t, $J_t = 7.55$ Hz, 1H), 7.95-7.86 (m, 3H), 7.75 (d, $J_d = 8.95$ Hz, 1H), 7.18 (d, $J_d = 8.95$ Hz, 1H), 6.54 (d, $J_d = 8.9$ Hz, 4H), 6.45 (d, $J_d = 8.9$ Hz, 4H), 5.44 (s, 2H), 5.23-5.18 (m, 2H), 3.96-3.92 (m, 5H), 3.91-3.89 (m, 2H), 3.81-3.61 (m, 8H), 3.56-3.54 (m, 2H), 3.37 (s, 3H), 2.82-2.77 (m, 2H), 1.90 (m, 2H), 1.69-1.67 (m, 4H), 1.42-1.27 (m, 12H); **¹³C NMR** (75 MHz, CDCl_3 , 25°C): δ (ppm) = 171.1, 165.1, 158.2, 157.6, 140.7, 139.1, 132.87, 128.47, 124.86, 121.81, 114.31, 73.13, 71.89, 71.12, 79.72, 70.6, 67.1, 65.5, 59.0, 49.3, 29.1, 28.2, 25.3; **IR** (KBr, cm^{-1}): 3569, 3317, 3066, 2844, 1899, 1727, 1566, 1496, 1375, 1254, 842; **MS (+EI)**: (m/z): Calcd for $\text{C}_{45}\text{H}_{58}\text{N}_4\text{O}_9\text{Pd}$; 905.38; found: 905.3 $[\text{M}]^+$ and 906.3 $[\text{M}+\text{H}]^+$, **Anal.** Calcd. for $\text{C}_{45}\text{H}_{58}\text{N}_4\text{O}_9\text{Pd}$: C, 59.70; H, 6.46, N, 6.19 found; C, 59.48; H, 6.49, N, 6.17.

General synthetic protocol for mesoporous silica MCM-41 gated with Pd(II)-metalated macrocycle

Mesoporous silica nanoparticles (MCM-41) were prepared according to well-established literature sol-gel procedures.²⁶ Cetyltrimethylammonium bromide CTAB (1.0 g, 2.74 mmol, 1.0 equiv) was dissolved in a mixture of deionized millipore H_2O (500 mL) and 2M NaOH (3.5 mL), and the solution was stirred under N_2 atmosphere and heated to constant temperature of 80°C. TEOS (5.2 mL) was then added slowly to the solution and aged at 80°C for 2 h. The solution was turned to opaque from initial clear solution, then the nanoparticles were centrifuged and washed thoroughly with MeOH and H_2O in order to remove CTAB. Subsequently, the as-synthesized particles were suspended in MeOH (120 mL) and hydrochloric acid (3.5 mL). The solution was refluxed for 16 h to remove the CTAB template completely, and the **MSNPs** classified

as MSN-1 were collected by centrifugation. The product was washed thoroughly with MeOH and H_2O and dried under vacuum for 24 h. Successful template removal by the chemical method was confirmed by shifts in bragg XRD peaks and increased volume of N_2 adsorption. The resulting **MSNs** were fully characterized using XRD, BET, SEM, TEM, IR and solid state CP-MAS NMR analysis.

3-Isocyanatopropyltriethoxysilane (ICPES) functionalized nanoparticles SN1s:

Surfactant removed nanoparticles were derivatized with ICPES initially using a modified chemical grafting method. Nanoparticles **MSNs** (300 mg) were suspended in anhydrous toluene (45 mL), and 3-ICPES (120 μL) was added to the solution. The reaction mixture was stirred at ambient temperature under an atmosphere of N_2 for 24 h. The isocyanato-functionalized nanoparticles **SN1s** were isolated by centrifugation, washed with toluene and MeOH, and dried under vacuum.

Pyridyl stalk functionalized nanoparticles SN2s:

Isocyanato-functionalized nanoparticles **SN1s** (200 mg) were suspended in anhydrous toluene (60 mL), and (6-(2,5,8,11-tetraoxadodecyl)pyridin-2-yl)methanol **3** (0.081 g, 0.28 mmol) was then added to the solution. The reaction mixture was stirred under reflux overnight under an atmosphere of N_2 . The pyridyl stalk functionalized nanoparticles **SN2s** were obtained by centrifugation, washed with toluene and MeOH, and dried under vacuum.

Pseudorotaxanated nanoparticles SN3s:

In view of control experiments, pyridyl stalked nanoparticles **SN2s** (50 mg) were suspended in a mixture of anhydrous solution $\text{CHCl}_3/\text{CH}_3\text{CN}$ (15 mL, 8:2, v/v) and macrocycle Pd complex **MPd** (20 mg) was then added to the solution. The reaction was agitated for 4 h under an atmosphere N_2 . The pseudorotaxanated nanoparticles **SN3s** were collected by centrifugation, washed with CHCl_3 , CH_3CN and MeOH to remove an excess of non-threaded macrocycle, and dried under vacuum.

Cargo loading and capping of nanoparticles SN4s:

To assess the efficacy of the present nanovalve system, the pores of pyridyl stalked **MSNs** were diffusion filled with cargo molecules by soaking the nanoparticles **SN2s** (15 mg) in fluorescein aqueous solution (5 mL, 0.5 mM) for 18 h. The pore-filled **MSNs** were then collected by centrifugation and re-dispersed in a mixture of $\text{CHCl}_3/\text{CH}_3\text{CN}$ (3 mL, 8:2, v/v) solution and then macrocycle-Pd metal complex (2 mL, 40 mM) was added to close the gate via covalent metal coordinated template effect. After 24 h of stirring, the surface-adsorbed dye molecules and excess macrocycle complex were washed using CHCl_3 , CH_3CN and water successively and removed by centrifugation to yield pore-filled square planar Pd(II)-template gated-nanovalves **SN4s**.

Control cargo releasing studies from pore filled Pd(II) metal template gated-nanovalves SN4s:

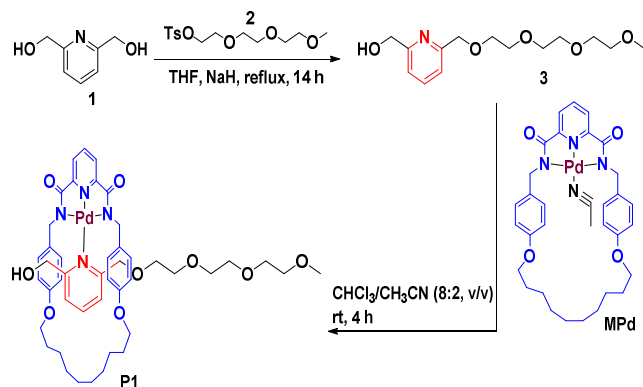
In view of dye releasing experiments 500 μL of as-prepared dye-loaded Pd(II)-templated nanovalves (2 mg/mL) were taken in quartz vial and diluted to 5 mL with PBS buffer (pH 7.4) under gentle stirring. To operate the Pd(II)-templated nanovalve, above solutions were treated with or without TBACN (5 mM). Simultaneously, the supernatant solutions were excited at 488 nm and the emission

maxima of releasing dyes at 516 nm were monitored as a function of time to produce a release profile.

Results and discussion

Preparation and characterization of organic stalk and MSNs:

Inspired by our early success in designing functional MIMs²⁷ and to get most out of the mechanized MSNs, herein we synthesized a monodentate pyridyl stalk **3** and macrocycle complex **MPd** with a tridentate 2,6-dicarboxyamidopyridine unit. Moreover, to mimic the working mechanism of functional organic group in this report, we prepared cyanide stimulus responsive pseudorotaxane **P1** as shown in the Scheme 1. First pyridine-2,6-diyl dimethanol **1** was reacted with 2-(2-(2-methoxyethoxy)ethoxy)ethyl 4-methylbenzenesulfonate **2** in tetrahydrofuran (THF) using NaH as deprotonating agent to afford mono hydroxyl organic stock **3** in a moderate yield. The selective mono hydroxylated derivative attached via carbamate linker to solid silica support.



Scheme 1 Synthesis of organic stalk **3** and pseudorotaxane **P1**.

In view of creating smart supramolecular nanovalves, we explored the conventional nanostructured silica (MCM-41) as a dual platform, such as solid supports for switchable molecular machines, and as a nano-container for the guest molecules which are trapped and then eventually released on demand. The synthesis of **MSNs** was carried out by a well-established sol-gel procedure²⁶ using NaOH as morphology catalyst and CTAB as a template directing agent to yield the self-assembled hierarchical nanoscale passageways. The surfactant template was removed by a modified solvent extraction method. As illustrated in Fig. 2a the SEM image shows that the nanostructured silica has a mean diameter of 90-120 nm with a near-spherical shape and a smooth surface. TEM, XRD and N₂ adsorption-desorption measurements at 77 K were probed further to confirm the morphology and porosity of **MSNs**. As shown in Fig. 2b the TEM image clearly verified the existence of a two-dimensional hexagonal mesoporous structure. Small-angle XRD image presented in Fig. S1 further affirmed the presence of mesoscopic hierarchy in the resulting hexagonal pores with a d_{100} spacing of about 4.0 nm. According to the IUPAC nomenclature, N₂ adsorption-desorption isotherm of the present material (Fig. S2a) could be classified as a type IV isotherm. Current **MSNs** exhibited a high BET surface area of 1155 m²g⁻¹. Further, Barret-Joyner-Halenda (BJH) analysis indicates that the material pore size distribution (PSD) is narrow and centred at 2.5 nm, as shown in Fig. S2b.

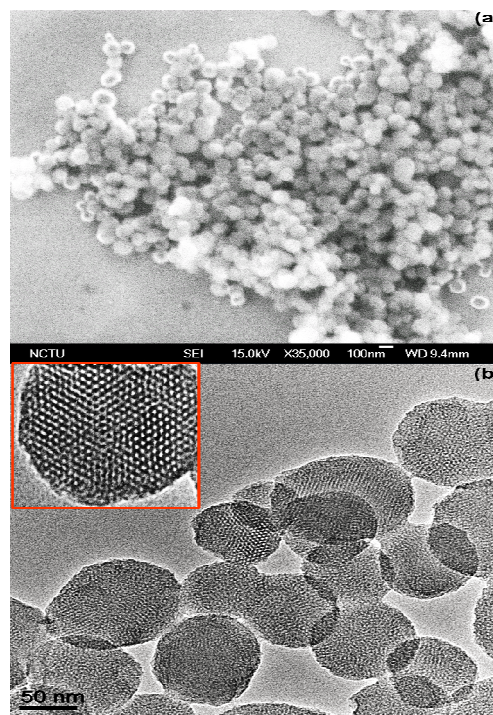


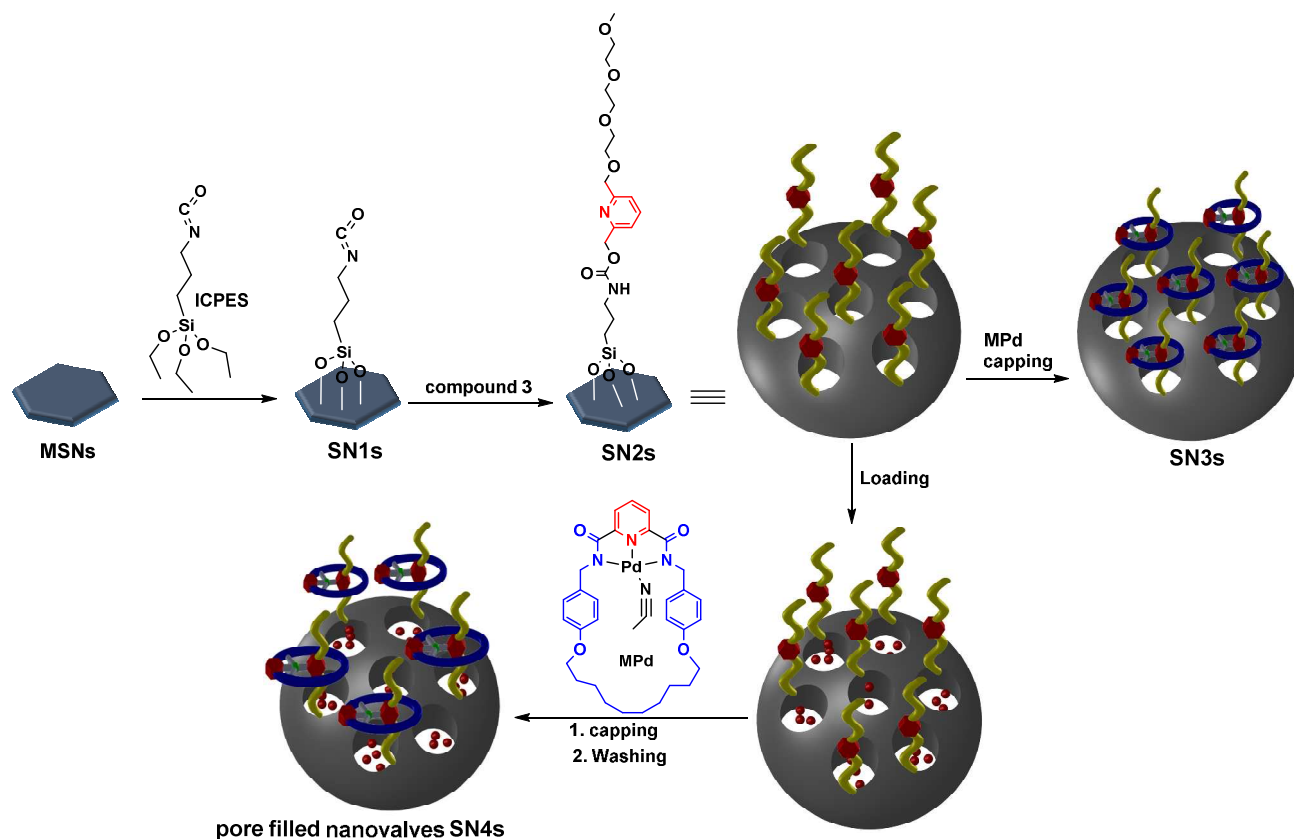
Fig. 2 (a) and (b) FE-SEM and HR-TEM micrographs of mesoporous silica nanoparticles **MSNs**, respectively; Inset in (b) is an enlarged portion to visualize mesopores.

These results clearly suggested that the present system has highly ordered nanopores, which are large enough to trap high contents of dye molecules, and also assists cargos to travel in and out of the **MSNs**. Moreover, nanopores were yet small enough to be clogged by organic macrocyclic molecules of interest, such as **MPd**.

Fabrication of mechanized **MSNs**:

Exquisite stimulus responsive nature of MIMs has long been prompting and thus chemically allowed to build myriads of nanovalves by utilization of weak non-covalent interactions.¹⁴⁻¹⁸ We developed a simple and yet an intelligent nanovalve system in this report by exploring Pd(II)-based square planar metal geometry as a capping agent. Operations of an archetype supramolecular nanovalves are often relied on the movable machineries grafted onto orifices of **MSNs**. However, nanovalve system should be ideal enough to avoid premature leakages and hence allow easy passages of cargos under anion cyanide stimuli. To accomplish this task, initially **MSNs** were functionalized with ICPES to create anchoring points for organic stalks. Mono-dentate pyridyl derivative **3** was grafted onto MCM-41 surface using a carbamate linkage in toluene solution as shown in Scheme 2. In order to finalize the whole fabrication process, **MSNs** were further loaded with cargos and subsequently capped with macrocycle-Pd complex **MPd**. For control releasing studies, silica materials **SN2s** were capped directly with macrocycle to afford **SN3s**.

The successful functionalization of organic stalks were confirmed by SEM imaging and EDX spectrometry analyses. As depicted in Fig. S3, the morphologies of silica **SN3s** were unperturbed after organic functionalization and showed well-preserved mechanical robustness. Explicit elemental mapping images further corroborate the existence of well dispersed Pd and N elements, which were instigated from organic stems on



Scheme 2 Synthesis of the square planar Pd(II)-template gated nanovalves SN4s.

silica surface. XPS and solid state CP-MAS NMR spectroscopies were further probed to confirm the surface functionalization. XPS spectra (Fig. S4) clearly verify the presence of C_{1s} (287.7 eV), N_{1s} (403.0 eV) and N_{2p} (133.9 eV), Pd 3d_{3/2} (345.9 eV) and 3d_{5/2} (335.6 eV) along with Si and O elements. As depicted in ²⁹Si CP-MAS NMR spectrum of **SN3s** (Fig. S5a), the corresponding resonance signals at -109.0, -100.1 and -91.2 ppm could be assigned to Q⁴, Q³ and Q² bands of silica surface.²⁸ Moreover, pertained resonance signals at -64.6 and -56.6 ppm denoted the T-series di (T2) and mono (T1) functionalized Si-C linkages, respectively, in Fig. S5b. As shown in Fig. S5c, ¹³C CP-MAS NMR spectrum of **SN3s** shows two characteristic weak and strong carbonyl peaks at 172.1 and 160.5 ppm, respectively, and one corresponding weak aromatic peak at 122.2 ppm, along with several strong aliphatic peaks in the region of 80-20 ppm. These results lucidly support the successful grafting of Pd-metal templated nanogate stalks on mesoporous orifices.

Furthermore, we carried out FT-IR and Zeta potential measurements on all nanostructured materials in this study. In Fig. S6a, each step of MSNs was compared to deduce effective organic grafting. The noticeable disappearance of C-H stretching peaks at 2962 and 2843 cm⁻¹ in MSNs in comparison with those of nanoparticles containing CTAB clearly denoted the optimal removal of surfactant-templating after acid extraction. Moreover, it indicates high surface silanol density owing to the aqueous synthetic conditions of silica particles as also suggested by Zink *et al.*¹⁹ In addition to weak C-H stretching peaks at 2954 and 2845 cm⁻¹, we noticed (see Fig. S6b) a

carbonyl stretching peak at 1642 cm⁻¹ and a N-H bending vibration band at 1439 cm⁻¹ for **SN3s** (pink line). Observable IR spectral changes within the region of 1800 to 1200 cm⁻¹ clearly indicate effective organic functionality in each stage. Furthermore, to our delight the complete transformation of zeta potential values from initial -40.7 mV of bare MCM-41 nanoparticles to final 32.1 mV of **SN3s** was observed in zeta potential measurements (see details in Table S1). These results obviously attest the effective grafting of nanogate stalks on silica surface pore openings. To further assess the surface density of Pd(II)-templated nanovalves on surface of MSNs and to know the dye loading capacity of current nanovalves, we conducted thermogravimetric analysis (TGA) of isocyanate linked nanoparticles **SN1s**, **SN3s** and dye loaded nanovalves **SN4s**. The Pd(II)-templated gate surface density and dye loading capacity of nanovalves **SN4s** are estimated to be 0.055g/g and 0.180 g/g, respectively (see Fig. S7). The high dye loading content could possibly be raised along with its inevitable humectant nature of long-standing dye loaded nanovalves.

Cyanide-responsive control releasing behaviour of Pd nanovalves SN4s:

To create a metal template nanovalve system, a square planar Pd(II)-templated pseudorotaxane was designed as a gate-keeper, which could be effectively demetalated and eventually pores were opened by the aqueous cyanide stimuli. To further

enhance aqueous solubility and to allow easy passage of macrocycle (acted as a primary ligand) over thread, pyridine-2,6-diylidimethanol was selectively alkylated with 2-(3-(2-methoxyethoxy)propoxy)ethanol unit. The demetalation process in this design was perceived as the affinity of Pd(II) metal for cyanide, which was high and efficient under working conditions as suggested by previous reports.^{25,29}

Prior to activate these nanovalves, we are intrigued to check the indispensable pseudorotaxane formation analyzed by ¹H NMR spectra of individual components. To this end, we compared the NMR spectra of free macrocycle, macrocycle and thread (1:1 mixture, free thread and pseudorotaxane. As depicted in the Fig. 3, we observed upfield chemical shifts for aromatic macrocycle protons **B**, **D** and **E** in pseudorotaxane compared with free macrocycle along with the disappeared amide proton **C**.

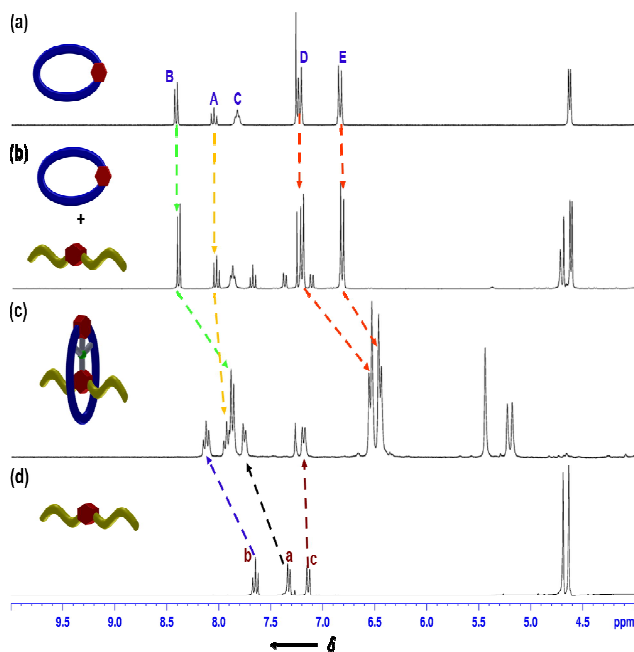


Fig. 3 ¹H NMR (CDCl₃, 300 MHz, 25°C) stock plot. (a) free macrocycle (3mM), (b) macrocycle and organic stack 1:1 mixture, (c) pseudorotaxane **P1** (3mM) and (d) organic stack **3** (3 mM). The alphabetical assignments are corresponding to lettering shown in Fig.1b.

Simultaneously, we noticed downfield shifts of thread protons **a** and **b**, hence these results clearly attested the effective pseudorotaxanation via a square planar Pd(II)-template formation between stacks and wheels. Conventionally, nanovalves were organized by using weak non-covalent interactions between the matching pieces. However, ideal topological cavities inspired by nature and metal geometry using stoichiometric metal template approaches have long been revolutionized the outcome of MIMs.

To get a better insight into the effects of anionic triggers on nanovalves and to mimic the nanovalve working function, we initially employed ¹H NMR titration of pseudorotaxane **P1** with CN⁻, as well as commonly encountered other monovalent anions, such as F⁻, Cl⁻, N₃⁻ and OAc⁻ with 4.0 equiv of respective tetrabutylammonium salts (see Fig. S8). Interestingly, no other tested anions exhibited significant spectroscopic changes except CN⁻. By considering this visible NMR changes, further titrations were conducted with CN⁻.

Upon the progressive addition of CN⁻, significant up-field shifts for axle protons **a**, **b** and **c** and noticeable down-field shifts for macrocycle protons **A**, **B** along with splitted resonances for protons **D** and **E** at 1 equiv of CN⁻, which were almost identical to chemical shifts as displayed in the mixture of axle and wheel shown in Fig 4a-e. To our delight, we noticed a regenerated amide resonance peak **C** upon the addition of 2 equiv CN⁻. On further addition, both of the axle and macrocyclic protons were splitted further with marginal up-field shifts along with precipitated tetrabutylammonium salts. Based on these ¹H NMR results, we infer that CN⁻ could be selectively reactive with Pd(II)-templated pseudorotaxane **P1** to free the wheels and axles apart. Moreover, splitted resonances for wheel and axle protons at higher concentrations of CN⁻ could be ascribed as the molecular asymmetric environment generated in situ owing to free amide macrocycle and some of unreacted wheel part coupling on NMR time scale.

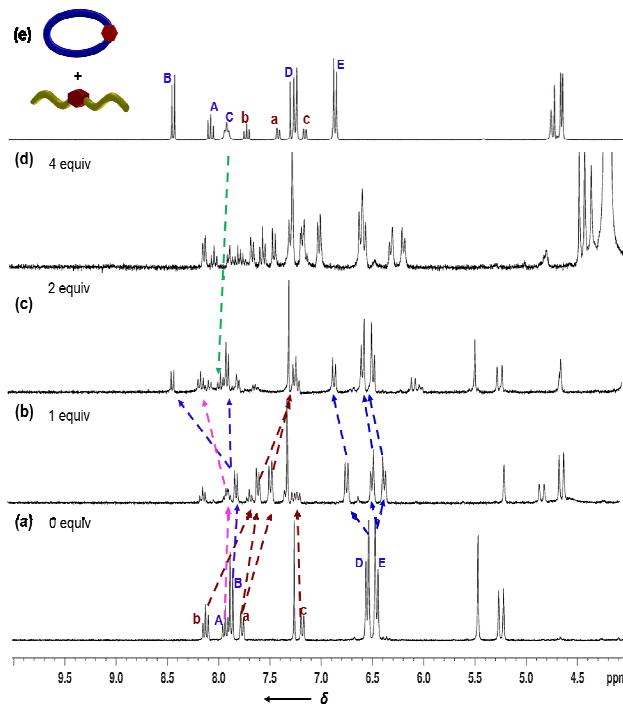


Fig. 4 Changes in ¹H NMR spectra (a-d) (CDCl₃, 300 MHz, 25°C) of pseudorotaxane **P1** (3 mM) with the addition of TBACN (in CD₃OD, 0-4 equiv) and (e) 1:1 mixture of macrocycle and organic stack. The alphabetical assignments are corresponding to lettering shown in Fig.1b.

To further investigate the efficacy of this nanovalve system, owing to the exceptional luminescence property of **FDS** we employed this dye as a cargo in this study. As mentioned above, guest dye molecules loaded into mesopores were conducted and washed extensively with the appropriate solvent until no guest molecules in the solution were detected. Morphologies of guest loading of Pd(II)-templated nanovalves **SN4s** were monitored further by HR-TEM analyses, in which we noticed unperturbed morphology with an identical spherical shape to that of initial **MSNs** as shown in Fig. S9. This result lucidly indicates the well confinement of guest molecules within the mesopores. To execute the operation and to verify the cyanide concentration effects on release function, dye loaded Pd(II)-template gated-nanovalves were taken in quartz cuvette and diluted to 5 mL with PBS buffer solution and agitated slowly so as to maintain

this homogenous solution throughout the operation. The assessment of dye loading and releasing percentile characteristics^{20,30} were monitored by using UV/Vis and PL changes as shown in Fig S10. To trigger the releasing event, cyanide stimulus was added and then the resulting solution concentration (excluding MSNs) was tracked by fluorescence intensity measurements of FDS at 516 nm with an exciting wavelength of 488 nm. We noticed an almost flat baseline at 516 nm prior to the activation of nanogate, which affirmed the no premature leakages through closed nanogate system.

Further, we screened the effects of the cyanide concentration on the nanogate releasing function, in which upon the initial addition of TBACN, we noticed marginal fluorescence proliferation with release percentile values of 28 and 32 at TBACN concentrations of 0.5 mM and 2 mM, respectively (see Fig. S11). Moreover, the continual plateau of release profile suggested that the demetalation process was not completed as some of the nanogates could not be demetalated enough. Based on this naked eye clue, we further carried out the release study with 5 mM of TBACN, in which we noticed significant increases in the fluorescence intensities owing to the releases of metal templates and simultaneous escapes of dye molecules into the solution as shown in Fig. 5. However, in the release experiment with a high cyanide concentration of 10 mM, we noticed an instant naked-eye observable increase in fluorescence of supernatant solution with precipitated salts and consistent with our aforementioned ¹H NMR titration measurements. We tested further the effects of thiol groups on the releasing function (see Fig. S11), in which we noticed a trivial response under the thiol group trigger. Thus, the present nanogates could selectively be triggered under cyanide stimuli.

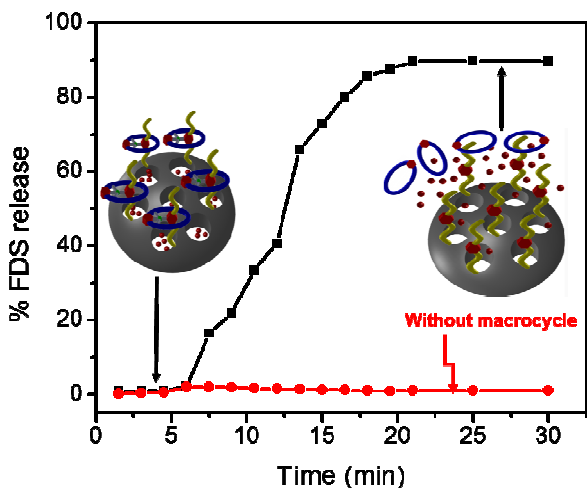


Fig. 5 The FDS release profiles of MCM-41 mechanized with Pd(II)-template gated-nanogates SN4s (black line) under cyanide trigger (5 mM) and the control experiment without macrocycles SN2s (red line).

To further ensure the demetalation of macrocycle being a pivotal step in opening the nanogate, we attached organic stacks to nanoparticles SN2s without macrocycles to screen the control releasing phenomenon. The assessment of releasing FDS guest in the control system was conducted as mentioned in the above protocol. However, a negligible dye releasing characteristics from the control system (i.e., nanoparticles SN2s without macrocycles) was observed upon the addition of

TBACN as shown in Fig. 5. As the stalks were not ideal enough to block the mesopores, the pores were not able to trap FDS molecules and thus all guest molecules escaped eventually prior to their activation. Thus the insignificant dye releasing characteristics in the case of SN2s may be attributed to residual surface-adsorbed dye molecules.

To know the blocking capability of macrocycles in reversible diffusion, we first capped the organic stalk nanoparticles SN2s with macrocycles and then treated with guest molecules to afford mechanized nanoparticles SN3s (with FDS molecules outside of pores). In assessment of releasing studies, we noticed a marginal fluorescent intensity enhancement from the resulting solution upon triggered with TBACN as depicted in Fig. S12a. We reasoned this observation as some of the mesopore orifices were not sealed completely owing to the imperfect coverage of capping linkers or macrocycles and hence some of the guest molecules were diffused into pores based on statistical basis and escaped upon activation.

It is crucial to monitor that, whether the nanogate operated via an anticipated mechanism or induced by an artifact of the working condition. In view of confirming the proposed mechanism, we screen the effect of solution pH on the overall efficacy of the nanogate. When the pH value of SN4s nanoparticle solution was adjusted to acidic condition (pH 2; see Fig. S12b), we noticed an almost flat baseline of release profile which verified that the lowering of pH could not induce demetalation. However, we noticed a prolonged release profile with marginal increase in the fluorescent intensity of FDS dye solution as pH was adjusted to basic condition (pH 12, see Fig. S12c), which indicated hydroxide ion could induce the demetalation process. Therefore, in contrast to the cyanide stimulus the releasing capability under hydroxide was far below.

As suggested by previous reports,^{13,31} synthesizing MSNs with the optimal pore size and short covalent chain length between anchoring point on MSNs surface and gated stations will be crucial in accommodating dye indicators of interests and to control the loading as well as releasing functions. A cyanide stimulus thus can be used as regulator to open the pores of MSNs via demetalation process in this current Pd nanogate. In a pre-activated state of the nanogate, the guest dye molecules were confined within the interiors of pores by means of metal coordinated gates on stacks. Owing to Pd(II) propensity towards the cyanide, the coordinated macrocycle was demetalated by cyanide and concurrently allowed the slippage of macrocycle ligands over stacks and leading to the release of cargos from mesopores as illustrated in Figs. 1a and S13.

Conclusions

In this report, we have developed a facile nanogate system under aqueous media based on cyanide responsive demetalation of a square planar Pd(II) metal template over organic stalks to proceed deliberate cargo release. A modular capping strategy has been developed to fabricate nanogates that rely on metal coordinated complex formation between wheels and stacks with ideal topological geometries. Control releasing features of dye molecules from the mesopores of nanogates triggered by aqueous cyanide stimulus in solution was successfully demonstrated, which also can be useful to be applied to detect the anion concentration of toxic CN⁻ in a cyanide-contaminated system by releasing different cargo contents of fluorescent dye indicator (e.g. FDS). More unique catalytic and ion transporting abilities of this nanogate system can be further

developed. We believe that the present approach could stimulate to build easy and effective allosteric fashioned nanovalve systems with various metal templates, which can be triggered by different moieties to open the nanovalves responsively and then to release the desirable porous contents (such as drugs or dye indicators) sequentially.

Acknowledgements

This project was financially supported by the National Science Council of Taiwan (ROC) through funding (No. NSC 101-2113-M-009-013-MY2, NSC 102-2221-E-009-174 and 102-2811-M-009-073).

Notes and references

- M. Vallet-Regí, A. Rámila, R. P. del Real and J. Pérez-Pariente, *Chem. Mater.*, 2001, **13**, 308-311.
- (a) P. Ehrlich, Chemotherapeutische Trypanosomen studien. *Berliner Klinische Wochenschrift.*, 1907, **44**, 233-236 (in German); (b) K. Strebhardt and A. Ullrich, *Nat. Rev. Cancer*, 2008, **8**, 473-480.
- T. Yanagisawa, T. Shimizu, K. Kuroda and C. Kato, *Bull. Chem. Soc. Jpn*, 1990, **63**, 988-992.
- (a) C. T. Kresge, M. E. Leonowicz, W. J. Roth, J. C. Vartuli and J. S. Beck, *Nature* 1992, **359**, 710-712; (b) J. S. Beck, J. C. Vartuli, W. J. Roth, M. E. Leonowicz, C. T. Kresge, K. D. Schmitt, C. T. W. Chu, D. H. Olson and E. W. Sheppard, *J. Am. Chem. Soc.*, 1992, **114**, 10834-10843.
- (a) F. Hoffmann, M. Cornelius, J. Morell and M. Fröba, *Angew. Chem. Int. Ed.*, 2006, **45**, 3216-3251; (b) Y. Wan and D. Y. Zhao, *Chem. Rev.*, 2007, **107**, 2821-2860; (c) I. I. Slowing, J. L. Vivero-Escoto, B. G. Trewyn and V. S. Y. Lin, *J. Mater. Chem.*, 2010, **20**, 7924-7937.
- (a) I. I. Slowing, J. L. Vivero-Escoto, C. W. Wu and V. S. Y. Lin, *Adv. Drug Deliv. Rev.*, 2008, **60**, 1278-1288; (b) J. Shen, Q. He, Y. Gao, J. Shi and Y. Li, *Nanoscale.*, 2011, **3**, 4314-4322; (c) Q. He and J. Shi, *J. Mater. Chem.*, 2011, **21**, 5845-5855; (d) F. Tang, L. Li and D. Chen, *Adv. Mater.*, 2012, **24**, 1504-1534.
- (a) K. Mori, T. Yamaguchi, S. Ikurumi and H. Yamashita, *Chem. Commun.*, 2013, **49**, 10468-10470; (b) G. Zhang, P. Wang and X. Wei, *Catal. Lett.* 2013, **143**, 1188-1194.
- (a) X. Wan, S. Yao, H. Liu and Y. Yao, *J. Mater. Chem. A*, 2013, **1**, 10505-10512; (b) M. S. Moorthy, D. J. Sao, H. J. Song, S. S. Park and C. S. Ha, *J. Mater. Chem. A*, 2013, **1**, 12485-12496; (c) L. Wu, J. Wang, H. Sun, J. Ren and X. Qu, *Adv. Healthcare Mater.* 2014, **3**, 588-595.
- (a) Y. Chen, H. Chen and J. Shi, *Adv. Mater.*, 2013, **25**, 3144-3176; (b) Y. Chen, H. Chen and J. Shi, *Exp. Opin. Drug Deliv.* 2014, **11**, 917-930.
- (a) B. G. Trewyn, I. I. Slowing, S. Giri, H.-T. Chen and V. S. Y. Lin, *Acc. Chem. Res.*, 2007, **40**, 846-853; (b) J. L. Blin and M. Imperoclerc, *Chem. Soc. Rev.*, 2013, **42**, 4071-4082.
- (a) S. Chia, J. Cao, J. F. Stoddart and J. I. Zink, *Angew. Chem. Int. Ed.*, 2001, **40**, 2447-2451; (b) R. Hernandez, H. R. Tseng, J. W. Wang, J. F. Stoddart and J. I. Zink, *J. Am. Chem. Soc.*, 2004, **126**, 3370-3371; (c) T. D. Nguyen, H. R. Tseng, P. C. Celestre, A. H. Flood, Y. Liu, J. F. Stoddart and J. I. Zink, *Proc. Natl. Acad. Sci.*, 2005, **102**, 10029-10034.
- (a) S. Angelos, E. Johansson, J. F. Stoddart and J. I. Zink, *Adv. Funct. Mater.* 2007, **17**, 2261-2271; (b) K. K. Coti, M. E. Belowich, M. Liong, M. W. Ambrogio, Y. A. Lau, H. A. Khatib, J. I. Zink, N. M. Khashab and J. F. Stoddart, *Nanoscale*, 2009, **1**, 16-39; (c) M. Liong, S. Angelos, E. Choi, K. Patel, J. F. Stoddart and J. I. Zink, *J. Mater. Chem.*, 2009, **19**, 6251-6257; (d) M. M. Boyle, R. A. Smaldone, A. C. Whalley, Y. Y. Botros and J. F. Stoddart, *Chem. Sci.*, 2011, **2**, 204-210.
- (a) M. W. Ambrogio, C. R. Thomas, Y. L. Zhao, J. I. Zink and J. F. Stoddart, *Acc. Chem. Res.*, 2011, **44**, 903-913; (b) Z. Li, J. C. Barnes, A. Bosoy and J. F. Stoddart, *Chem. Soc. Rev.*, 2012, **41**, 2590-2605; (c) Y. W. Yang, Y. L. Sun and N. Song, *Acc. Chem. Res.*, 2014, **47**, 1950-1960.
- (a) K. Patel, S. Angelos, W. R. Dichtel, A. Coskun, Y. W. Yang, J. I. Zink and J. F. Stoddart, *J. Am. Chem. Soc.*, 2008, **130**, 2382-2383; (b) D. P. Ferris, Y. L. Zhao, N. M. Khashab, H. A. Khatib, J. F. Stoddart and J. I. Zink, *J. Am. Chem. Soc.*, 2009, **131**, 1686-1688; (c) M. W. Ambrogio, T. A. Pecorelli, K. Patel, N.M. Khashab, A. Trabolsi, H. A. Khatib, Y. Y. Botros, J. I. Zink and J. F. Stoddart, *Org. Lett.*, 2010, **12**, 3304-3307; (d) M. Xue, D. Cao, J. I. Zink and J. F. Stoddart, *Nanoscale*, 2012, **4**, 7569-7574; (e) C. Wang, Z. Li, D. Cao, Y.-L. Zhao, J. W. Gaines, O. A. Bozdemir, M. W. Ambrogio, M. Frasconi, Y. Y. Botros, J. I. Zink and J. F. Stoddart, *Angew. Chem. Int. Ed.*, 2012, **51**, 5460-5465; (f) T. M. Guardado-Alvarez, L. Sudhadevi, M. M. Russell, B. J. Schwartz and J. I. Zink, *J. Am. Chem. Soc.*, 2013, **135**, 14000-14003; (g) M. Xue and J. I. Zink, *J. Am. Chem. Soc.*, 2013, **135**, 17659-17662; (h) J. A. Krings, B. Vonhören, P. Tejeder, V. Siozios, M. Peterlechner and B. J. Ravoo, *J. Mater. Chem. A*, 2014, **2**, 9587-9593.
- (a) S. Angelos, Y. W. Yang, K. Patel, J. F. Stoddart and, J. I. Zink, *Angew. Chem. Int. Ed.*, 2008, **47**, 2222-2226; (b) N. M. Khashab, M. E. Belowich, A. Trabolsi, D. C. Friedman, C. Valente, Y. Lau, H. A. Khatib, J. I. Zink and J. F. Stoddart, *Chem. Commun.*, 2009, 5371-5373; (c) S. Angelos, Y. W. Yang, N. M. Khashab, J. F. Stoddart and, J. I. Zink, *J. Am. Chem. Soc.*, 2009, **131**, 11344-11346; (d) S. Angelos, N. M. Khashab, Y. W. Yang, A. Trabolsi, H. A. Khatib, J. F. Stoddart and J. I. Zink, *J. Am. Chem. Soc.*; 2009, **131**, 12912-12914; (e) C. R. Thomas, D. P. Ferris, J. H. Lee, E. Choi, M. Y. Cho, E. S. Kim, J. F. Stoddart, J. S. Shin, J. Cheon and J. I. Zink, *J. Am. Chem. Soc.*, 2010, **132**, 10623-10625; (f) M. D. Wang, T. Chen, C. D. Ding and J. J. Fu, *Chem. Commun.*, 2014, **50**, 5068-5071.
- (a) T. D. Nguyen, K. C. F. Leung, M. Liong, C. D. Pentecost, J. F. Stoddart and J. I. Zink, *Org. Lett.* 2006, **6**, 3363-3366; (b) K. C. F. Leung, T. D. Nguyen, J. F. Stoddart and J. I. Zink, *Chem. Mater.*, 2006, **18**, 5919-5928.
- (a) Y. L. Sun, Y. Zhou, Q. L. Li and Y. W. Yang, *Chem. Commun.*, 2013, **49**, 9033-9035; (b) H. Li, L. L. Tan, P. Jia, Q. L. Li, Y. L. Sun, J. Zhang, Y. Q. Ning, J. Yu and Y. W. Yang, *Chem. Sci.*, 2014, **5**, 2804-2808.
- (a) Y. L. Sun, Y. W. Yang, D. X. Chen, G. Wang, Y. Zhou, C. Y. Wang and J. F. Stoddart, *Small*, 2013, **9**, 3224-3229; (b) Y. Zhou, L. L. Tan, Q. L. Li, X. L. Qiu, A. D. Qi, Y. Tao and Y. W. Yang, *Chem. Eur. J.* 2014, **20**, 2998-3004.
- D. Tarn, M. Xue and J. I. Zink, *Inorg. Chem.*, 2013, **52**, 2044-2049.
- S. Wu, Q. Deng, X. Huang and X. Du, *ACS Appl. Mater. Interfaces*. 2014, **6**, 15217-15223.
- S. R. Gayam and S. P. Wu, *J. Mater. Chem. B.*, 2014, **2**, 7009-7016.
- (a) F. Bezanilla and C. M. Armstrong, *J. Gen. Physiol.*, 1972, **60**, 588-608; (b) J. P. Changeux and S. J. Edelstein, *Science* 2005, **308**, 1424-1428; (c) D. C. Camerino, J. F. Desaphy, D. Tricarico, S. Piermo and A. Liantonio, *Adv. Genet.*, 2008, **64**, 81-145; (d) A. S.

- Verkman and L. J. Galletta, *Nat. Rev. Drug. Discov.* 2009, **8**, 153-171.
- 23 S. Abada, A. Lecointre, M. Elhabiri and L. J. Charbonniere, *Dalton Trans.*, 2010, **29**, 9055-9062.
- 24 R. K. Roy, E. B. Gowd and S. Ramakrishnan, *Macromolecules*, 2012, **45**, 3063-3069.
- 25 A. M. Fuller, D. A. Leigh, P. J. Lusby, A. M. Z. Slawin and D. B. Walker, *J. Am. Chem. Soc.*, 2005, **127**, 12612-12619.
- 26 (a) M. Liong, J. Lu, M. Kovoichich, T. Xia, S. G. Ruehm, A. E. Nel, F. Tamanoi and J. I. Zink, *ACS Nano*, 2008, **2**, 889-896; (b) Y. L. Zhao, Z. Li, S. Kabehie, Y. Y. Botros, J. F. Stoddart and Z.I. Zink, *J. Am. Chem. Soc.*, 2010, **132**, 13016-13025.
- 27 (a) M. V. R. Raju and H. C. Lin, *Org. Lett.*, 2013, **15**, 1274-1277; (b) M. V. R. Raju, P. Raghunath, M. C. Lin and H. C. Lin, *Macromolecules*, 2013, **46**, 6731-6743; (c) M. V. R. Raju and H. C. Lin, *Org. Lett.*, 2014, **16**, 5564-5567.
- 28 J. Fu, T. Chen, M. D. Wang, N. W. Yang, S. N. Li, Y. Wang and X. D. Liu, *ACS Nano*, 2013, **7**, 11397-11408.
- 29 (a) R. D. Hancock and A. Evers, *Inorg. Chem.* 1976, **15**, 995-996; (b) J. M. Harrington, S. B. Jones and R. D. Hancock, *Inorg. Chem. Acta.*, 2005, **358**, 4473-4480.
- 30 D. Xiao, H. Z. Jia, J. Zhang, C. W. Liu, R. X. Zhuo and X. Z. Zhang, *Small*. 2014, **10**, 591-598.
- 31 (a) T. D. Nguyen, Y. Liu, S. Saha, K. C. F. Leung, J. F. Stoddart and J. I. Zink, *J. Am. Chem. Soc.*, 2007, **129**, 626-634; (b) H. Meng, M. Xue, T. Xia, Y. L. Zhao, F. Tamanoi, J. F. Stoddart, J. I. Zink and A. E. Nel, *J. Am. Chem. Soc.*, 2010, **132**, 12690-12697.